Applied Catalysis B: Environmental 163 (2015) 539–546

Contents lists available at ScienceDirect

Applied Catalysis B: Environmental

journal homepage: www.elsevier.com/locate/apcatb

Modeling of photocatalyatic process on synthesized ZnO nanoparticles: Kinetic model development and artificial neural networks

A.R. Amani-Ghadim [a,*], M.S. Seyed Dorraji [b,1]

[a] Department of Chemistry, Faculty of Science, Azarbaijan Shahid Madani University, P.O. box 83714-161, Tabriz, Iran
[b] Department of Chemistry, Faculty of Science, University of Zanjan, Zanjan, Iran

ARTICLE INFO

Article history:
Received 4 May 2014
Received in revised form 12 June 2014
Accepted 13 August 2014
Available online 21 August 2014

Keywords:
Photocatalyst
Elementary photocatalytic reactions
Electron-hole
Recombination
ANN

ABSTRACT

The kinetic modeling of organic pollutant photocatalytic degradation on synthesized ZnO nanoparticles was carried out. The photodegradation kinetic characteristics were investigated under different operational parameters including light intensity, initial organic concentration, ZnO content and pH. Based on the elementary photocatalytic reactions, the new kinetic model was established for prediction of photocatalytic degradation efficiency by taking into account the apparent first order rate constant, light intensity, initial organic concentration and ZnO content. The results demonstrated that the kinetic model could predict adequately photodegradation efficiency when high concentration of photo-induced hole-electron was considered. To compare the accuracy of obtained kinetic model, an empirical kinetic model as function of operational parameters and a 3-layer perceptron neural network were developed. The performance of three models was compared with experimental data by error functions and analysis of variance (ANOVA) calculation. The obtained results showed that three developed models are in good agreement with experimental data. It was also found that there is no significant difference among the developed kinetic, empirical kinetic and artificial neural network models. It was concluded that the kinetic model is developed based on the appropriate understanding from determining elementary reactions occurred in photocatalytic degradation of dye.

1. Introduction

Over the past few decades, advanced oxidation processes based on heterogeneous photocatalysts have received enormous consideration as the effective treatment technique for destruction of persistent organic pollutants because of strong oxidative active oxygen species generation during irradiation on photocatalysts [1–3]. Generally, in heterogeneous photocatalytic process, occurring of several photochemical reactions provides a powerful oxidizing media to destruct organic pollutants [2].

Among various semiconductors (TiO_2, ZnO, CdS, . . .) employed as photocatalyst, titanium dioxide (with band gap of 3.2 ev) has been widely utilized for photocatalysis and the decontamination of water-soluble organic compounds [4–8]. Although the application of TiO_2 in environmental remediation has been of great interest, zinc oxide could also be considered as effective and alternative photocatalyst due to lower production cost, comparable band gap (3.3 ev), relatively faster rate of reaction, safety and biodegradability [9–12].

A considerable amount of literature have reported the removal of various types of organic pollutants by ZnO photocatalyst [9,13–18]. These reported works have focused on the effects of operational parameters on the removal efficiency of various types of organics, chemical pathway, kinetics and immobilization of photocatalyst on special supports. However, there have been no reports about the modeling of organics degradation by ZnO photocatalyst. So, developing the efficient models for better optimization of photocatalytic process is necessary. The modeling of processes based on the kinetic studies is one of the best types of modeling methods because they are developed based on the correct understanding of occurred reactions in the process and effects of operational parameters. Photocatalytic systems are very complicated processes owing to the occurrence of various elementary reactions [19]. Since, the kinetic modeling of photocatalytic removal processes have a number of problems. In most studies, first-order kinetics (Eq. 1) has been widely utilized for kinetic expression of

* Corresponding author. Tel.: +98 412 4327500; fax: +98 412 4327541.
E-mail addresses: a.r_amani@yahoo.com (A.R. Amani-Ghadim), saeed_dorraji@yahoo.com (M.S.S. Dorraji).
[1] Tel: (+98) (241) (5152477), Fax: (+98) (241) (5152477)

http://dx.doi.org/10.1016/j.apcatb.2014.08.020
0926-3373/

Table 1
Characteristics of C. I. Acid Blue 9.

Structure	C.I. Number	Synonyms	Chemical formula	Chemical class	λ_{max} (nm)
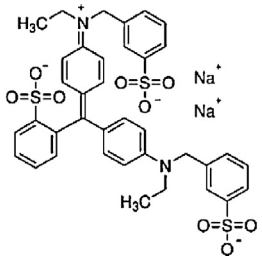	42090	Erioglaucine, Brilliant Blue FCF	$[C_{37}H_{34}N_2O_9S_3]^{2-}$, $2Na^+$	Triarylmethane	629

photocatalytic processes due to good agreement with experimental data [20]:

$$\frac{-dC}{dt} = k_{app} \times C \quad \rightarrow \quad \frac{c}{c_0} = \exp(-k_{app} \times t) \tag{1}$$

where C_0 is the initial concentration of pollutant, C is its concentration at time t and k_{app} is the first order rate constant. The relationship between first-order rate constant and initial pollutant concentration is commonly explained by Langmuir–Hinshelwood (L–H) model (Eq. 2) in photocatalytic process [21]:

$$\frac{-dC}{dt} = k_{app} \times C = \frac{k_r K_{ads} C}{1 + K_{ads} C_0} \tag{2}$$

In this equation, k_r and K_{ads} are the reaction rate constant and apparent equilibrium adsorption constant, respectively. According to L–H model, the rate constant depends on organic content and adsorption performance of photocatalyst [20]. Although, the L–H model has been successfully used in photocatalytic process, it must be noticed that the k_{app} vary with other operational parameters such as light intensity, pH and photocatalyst content. So, considering the mentioned parameters in the developing of kinetic model lead to obtain a relationship between k_{app} and effective factors.

As we know best, the reported works about the kinetic modeling of photocatalytic processes focus on kinetic study and developing kinetic models in which initial concentration and/or light intensity are considered in constant amount of photocatalyst [19,20,22–28]. Accordingly, in this paper, a new kinetic model is developed by considering the effect of initial organic concentration, reaction intermediates, light intensity (I) and ZnO content. In this way, the kinetic characteristics of photocatalytic degradation of Acid Blue 9 dye (as a model organic contaminant) in the presence of ZnO nanoparticles at different initial concentrations of dye, pH, light intensity and photocatalyst content were investigated. Then, based on the intrinsic elementary reactions, a novel kinetic model was developed by consideration of apparent first order kinetics and three effective parameters including initial contaminant concentration (C_0), light intensity (I) and ZnO content. Moreover, an empirical kinetic model and artificial neural network (ANN) were established to evaluate the accuracy of a developed kinetic model and intrinsic elementary reactions involved in kinetic model. ANNs are a non-linear and simplified mathematical models where its main idea has been achieved from neurological functioning of the brain [22–24]. They are able to recognize and reproduce the relationship between multiple inputs and output of systems. Due to not needing mathematical description of the phenomena involved in the process, artificial neural networks are appropriate and adequate for modeling of complicated processes such as photocatalytic decontamination process [25].

2. Material and methods

2.1. Materials

Zinc sulfate, hydrochloric acid and sodium hydroxide were of analytical reagent grade and were used as received. C. I. Acid blue 9 (AB9) was provided by Boyakhsaz Iran. Its structure and characteristics are given in Table 1. Distilled water was used throughout the work.

2.2. Preparation and characterization of ZnO nanoparticles

ZnO nanoparticles were prepared by a precipitation method [26]. In a typical procedure, $ZnSO_4.7H_2O$ was used as starting material and NaOH as the precipitant. NaOH solution was added dropwise to the vigorously stirred solution to adjust pH to about 7 and a large amount of white slurry was formed. The wet powder was dried at about 100 °C in air to form the precursor of ZnO. Finally, the precursor was calcined in air at a certain temperature (300 °C for 3 h) to produce the nano-sized ZnO photocatalyst.

The prepared ZnO nanoparticles were characterized using X-ray diffraction (XRD) (Simens D-5000 diffractometer, Cu K_α radiation, Germany). The XRD pattern of prepared ZnO nano particles (shown in Fig. S1 of the supporting information) matched with ICPDS file no. 36-1451 and the particles show hexagonal crystal system. Nine peaks appear at $2\theta = 31.8^o$, 34.6^o, 36.4^o, 47.7^o, 56.7^o, 63.4^o, 66.2^o, 68^o and 68.9^o, which correspond to (100), (002), (101), (102), (110), (103), (200), (112) and (210), respectively. It seems that the prepared ZnO nanoparticles possess a high crystallinity, since all the peaks are very sharp.

The surface morphology of zinc oxide nanoparticles was characterized by scanning electron microscopy (SEM) (VEGA\\TESCAN, Czech Republic). The size and morphology of the nanoparticles were characterized by transmission electron microscopy (TEM; CM120 Philips, Netherland) operated with a 120 kV electron beam. Fig. 1a and b shows SEM and TEM images of zinc oxide nanoparticles. The particles show spherical morphology. It is possible to observe ZnO nanoparticles with an average size of 50 nm (Fig. 1b). Gas sorption analysis (Brunauer–Emmett–Teller (BET) method) was carried out using a Quantachrome Chem BET. The result indicates that the specific surface area of prepared nanoparticles is about 16 $m^2\ g^{-1}$.

2.3. Procedure

For the UV/ZnO process, irradiation was carried out with a 30 W (UV-C) mercury lamp (Philips, Germany), which was put above a batch slurry reactor of 500 ml in volume. In all experiments, 100 ml of the AB9 solution containing appropriate quantity of the ZnO suspensions were used. The pH of solution values were adjusted

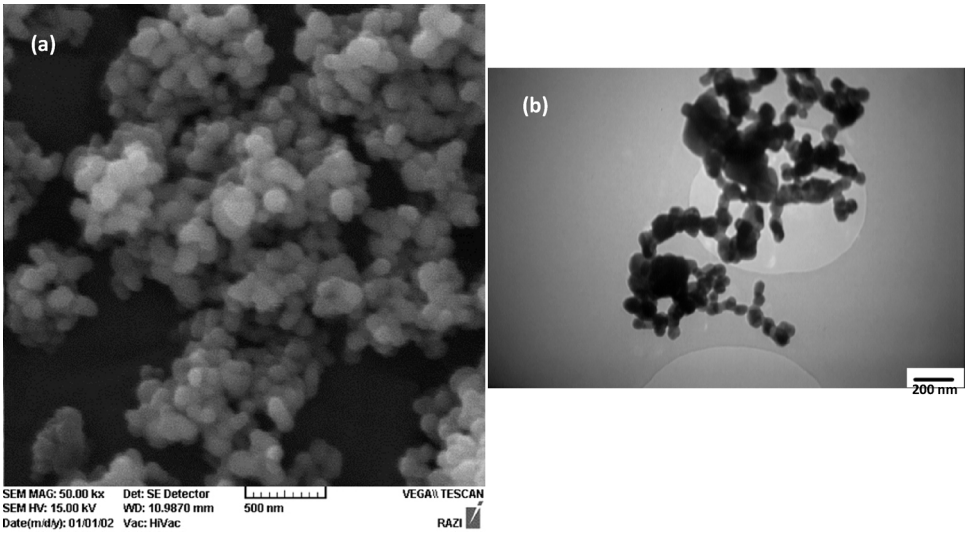

Fig. 1. SEM (a) and TEM (b) images of prepared ZnO nanoparticles.

at desired value by dilute NaOH and H_2SO_4 solutions and measured with pH meter (Philips PW 9422, Holland). The suspension was stirred for 30 min in the dark for the attainment of adsorption equilibrium. The distance between UV lamp and surface of solution was set in certain values to adjust the light intensity in the range of 8–16.3 W/m^2. Then, The UV lamp was switched on to initiate the reaction. The light intensity was measured using UV radiometer (Cassy Lab Company, Germany). The UV lamp was switched off for the control experiments that were carried out in the dark. During irradiation, agitation was maintained to keep the suspension homogenous, saturation of oxygen and increasing mass transfer coefficient. At specific time intervals, suspension was sampled and samples were filtered through a 0.2 μm membrane filter (Schleicher & Schuell, Germany). The concentration of AB9 in each sample was determined using a spectrophotometer (Perkin-Elmer 550 SE, USA) at λ_{max} = 629 nm and a calibration curve.

3. Results and discussions

3.1. The effects of operational parameters on photocatalytic degradation of AB9

The changes in the removal efficiency (X) of dye as a function of time during the adsorption of dye by ZnO in the dark, direct photolysis by UV irradiation without ZnO and photocatalytic degradation of dye (UV/ZnO) were demonstrated in Fig. 2. These experiments were carried out to show the photocatalytic performance of synthesized ZnO nanoparticles. The results revealed that the direct photodegradation of AB9 was negligible in the absence of ZnO. Removal of AB9 was less than 4% in the direct photolysis and adsorption by ZnO in the dark, which indicates that the observed high decomposition of AB9 in the UV/ZnO process is exclusively attributed to the photocatalytic reaction of the semiconductor particles.

In order to investigate the influence of the initial AB9 concentration, pH, light intensity and zinc oxide content in AB9 photocatalytic degradation, experiments were conducted with different values of parameters. A plot of $-\ln(C/C_0)$ versus time for all experiments has been shown in Fig. 3. It could be seen that the curves of AB9 degradation are well fitted with first-order kinetic equation. It must be mentioned that second-order kinetic equation ($1/C - 1/C_0$ vs. time) was examined for all experiments. The comparison of correlation coefficient (R^2) values, given in Table S1 of the supporting information, led us to consider the first order kinetics in photocatalytic degradation of AB9 because R^2 values for first-order kinetics were considerably higher than R^2 values related to second-order kinetic equation. Based on the results presented in Fig. 3, it is clear that the considered parameters have impressive effect on the removal efficiency. The degradation rate decreases with initial AB9 concentration increasing (Fig. 3a). As the concentration of organic content increases, the illuminated photons are absorbed by organic molecules; hence the absorption of photons by the photocatalyst decreases [20]. Based on the experimental results, k_{app} increased with increasing the ZnO content and light intensity up to 125 mg/L and 16.3 W/m^2, respectively (Figs. 3b and c). The investigation of pH effect showed that the removal efficiency of dye decreased with pH value (Fig. 3d). According to the literature, the decrease of AB9 degradation at alkaline pH could be explained by considering the surface charge of ZnO nanoparticles and dye. Repulsion occurs at alkaline pH because this AB9 and ZnO are negatively charged [27,28].

3.2. Kinetic model development for photocatalytic degradation

Generally, in photocatalytic degradation process, it is assumed that the hydroxyl radicals adsorbed on photocatalyst, aggress

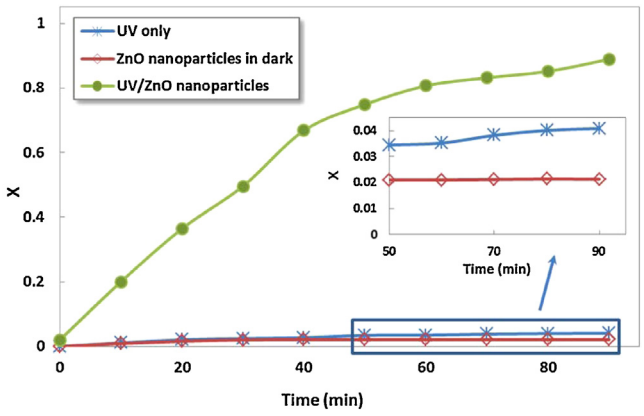

Fig. 2. Comparison of different processes including (a) adsorption by ZnO in dark, (b) direct photolysis by UV irradiation without ZnO and (c) photocatalytic degradation by UV light and ZnO nanoparticles in the removal of AB9 ($[AB9]_o$ = 20 mg/L, [ZnO] = 125 mg/L, pH = 6.5 and [L.I] = 11.2 W/m^2).

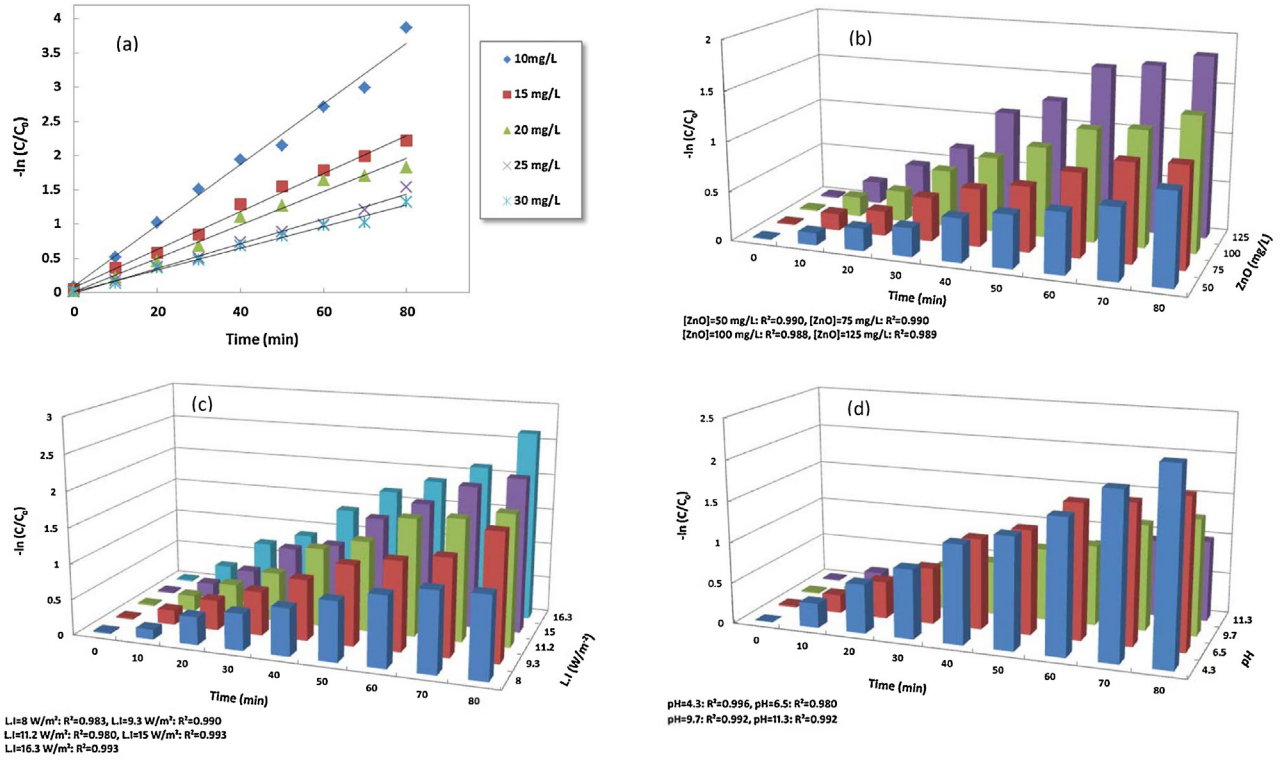

Fig. 3. Effect of (a) initial dye concentration, (b) ZnO content, (c) light intensity and (d) pH on the photocatalytic degradation of AB9. The value of the fixed variables to carry out experiments of series (a) [ZnO] = 125 mg/L, pH = 6.5 and [L.I] = 11.2 W/m^2 (b) ([AB9]$_o$ = 20 mg/L, pH = 6.5 and [L.I] = 11.2 W/m^2 (c) [AB9]$_o$ = 20 mg/L, [ZnO] = 125 mg/L and pH = 6.5 (d) [AB9]$_o$ = 20 mg/L, [ZnO] = 125 mg/L and [L.I] = 11.2 W/m^2.

adsorbed organics and destroy them. The elementary steps representing the proposed mechanism as well as related reaction equations are summarized in the following:

* Excitation

$$ZnO + hv \xrightarrow{k_1} h^+ + e^- \quad (3)$$

* Recombination:

$$h^+ + e^- \xrightarrow{k_2} heat \quad (4)$$

* Adsorption:

$$H_2O + S_{ZnO} \xrightarrow{k_3} H_2O_{ads} \quad (5)$$

$$OH^- + H^+ + S_{ZnO} \xrightarrow{k'_3} OH^-_{ads} + H^+ \quad (6)$$

$$Dye + S_{ZnO} \xrightarrow{k_4} [Dye]_{ads} \quad (7)$$

* Trapping:

$$H_2O_{ads} + h^+ + \xrightarrow{k_5} \cdot OH_{ads} + H^+ \quad (8)$$

$$OH^- + h^+ \xrightarrow{k_6} \cdot OH_{ads} \quad (9)$$

*Hydroxyl radical attack

$$\cdot OH_{ads} + [Dye]_{ads} \xrightarrow{k_7} [\text{colorless intermediate}] \quad (10)$$

$$\cdot OH_{ads} + [\text{colorless intermediate}] \xrightarrow{k_8} \text{inactive species} \quad (11)$$

*Hydroxyl radical deactivation

$$\cdot OH_{ads} + e^- \xrightarrow{k_9} OH^-_{ads} \quad (12)$$

$$\cdot OH_{ads} \xrightarrow{k_{10}} OH^-_{ads} + h^+ \quad (13)$$

From Eq. 10, the destruction of adsorbed organic dye is performed by adsorbed hydroxyl radicals. So, the rate equation of dye destruction (r_D) could be expressed as Eq. 14:

$$r_D = k'[\cdot OH]_{ads}[Dye] \quad (14)$$

where, k_7 and [Dye] are the rate constant of dye degradation and concentration of the adsorbed dye molecules, respectively. By considering the steady-state approximation for total concentration of hydroxyl radicals, [·OH] is constant and could be obtained by:

$$\frac{d[\cdot OH]}{dt} = k_5[h^+][H_2O]_{ads} + k_6[h^+][OH^-]_{ads} - k_7[\cdot OH][Dye]_{ads} - k_8[\cdot OH][\text{intermediates}]_{ads} - k_9[\cdot OH][e^-] - k_{10}[\cdot OH] \approx 0 \quad (15)$$

The rearrangement of Eq. 15 gives:

$$[\cdot OH] = \frac{(k_5[H_2O]_{ads} + k_6[OH^-]_{ads})[h^+]}{k_7[Dye]_{ads} + k_8[\text{intermediated}]_{ads} + k_9[e^-] + k_{10}} \quad (16)$$

Because the experiments carried out in neutral pH and this fact that water is solvent, it could be assumed that hydroxyl radicals are mainly formed via trapping the holes by adsorbed water molecules. Consequently, in Eq. 16, $k_6[OH^-]$ could be omitted and $k_5[H_2O]_{ads} = k_t$:

$$[\cdot OH] = \frac{k_t[h^+]}{k_7[Dye]_{ads} + k_8[\text{intermediated}]_{ads} + k_9[e^-] + k_{10}} \quad (17)$$

Eq. (17) includes unknown $[Dye]_{ads}$ and $[\text{intermediates}]_{ads}$ which are impossible to measure. Nevertheless, the following assumption could modify Eq. 17:

$$[Dye]_{ads} + [\text{Intermediates}] = [Dye]_0 \quad (18)$$

Table 2
Constants, SSE and RMSE of the developed kinetic models.

Developed model	Equation constants	Constants values	R^2	SSE	RMSE
$k_{app,LheC} = \frac{\beta_{L,1} I[ZnO]}{1+\beta_{L,2}[Dye]_0+\beta_{L,3} I[ZnO]}$	$\beta_{L,1} = k' \frac{k_1}{k_{10}}$	-1.02×10^{-5}	0.8283	2.294×10^{-4}	$\mathbf{4.372 \times 10^{-3}}$
	$\beta_{L,2} = \frac{k_7+k_8}{k_{10}}$	−0.04733			
	$\beta_{L,3} = \frac{k_9}{k_{10}} \frac{k_1}{k_t}$	−0.00047			
$k_{app,HheC} = \frac{\beta_{H,1} I^{1/2}[ZnO]^{1/2}}{1+\beta_{H,2}[Dye]_0+\beta_{H,3} I^{1/2}[ZnO]^{1/2}}$	$\beta_{H,1} = k' \left(\frac{k_t}{k_{10}}\right) \left(\frac{k_1}{k_2}\right)^{1/2}$	0.000472	0.9762	2.530×10^{-5}	$\mathbf{1.452 \times 10^{-3}}$
	$\beta_{H,2} = \frac{k_7+k_8}{k_{10}}$	0.036082			
	$\beta_{H,3} = \left(\frac{k_9}{k_{10}}\right) \left(\frac{k_1}{k_2}\right)^{1/2}$	−0.02494			

$$k_7[Dye]_{ads} + k_8[Intermediates]_{ads} = k_7([Dye]_0 - [Intermediates]) + k_8([Dye]_0 - [Dye]_{ads}) = (k_7 + k_8)[Dye]_0 - k_7[Intermediates] - k_8[Dye]_{ads} \approx (k_7 + k_8)[Dye]_0 \quad (19)$$

In fact, it is assumed that the term k_7[intermediates]–$k_8[dye]_{ads}$ is lower in comparison with $(k_7 + k_8)[Dye]_0$. On the other hand, the photogeneration of holes and electrons are equal. Accordingly, the concentrations of e^- and h^+ are equal. By substituting assumption 19 in Eq. 17 and dividing it by k_{10}, Eq. 20 is obtained:

$$[\cdot OH] = \frac{\frac{k_t}{k_{10}}[h^+]}{1 + \left(\frac{k_7+k_8}{k_{10}}\right)[Dye]_0 + \frac{k_9}{k_{10}}[h+]} \quad (20)$$

The concentration of photo-induced holes can be achieved by steady-state approximation as follows:

$$\frac{d[h^+]}{dt} = k_1 I[ZnO] - k_2[h^+][e^-] - k_5[h^+][H_2O]_{ads} - k_6[h^+][OH^-]_{ads} \approx 0 \quad (21)$$

By considering, $k_5[h^+][H_2O]_{ads} > k_6[h^+][OH^-]_{ads}$, $k_5[H_2O]_{ads} = k_t$ and $[h^+] = [e^-]$ assumptions:

$$k_1 I[ZnO] = k_2[h^+]^2 + k_t[h^+] \quad (22)$$

In literature, there are conflicting reports about Eq. 22. Some authors considered that trapping of valence band holes with water molecules could compete with recombination reaction [29–32]. In other words, they developed the kinetic model for photocatalytic degradation by the following assumption:

$$k_2[h^+] << k_t[h^+] \quad (23)$$

In contrast, in some reports, the kinetic model was developed with fast recombination assuming [19,20,33] (Eq. 24).

$$k_2[h^+]^2 >> k_t[h^+] \quad (24)$$

Rothenberger [34] showed that at very low electron-hole concentration, trapping of holes with water molecules could compete with charge carriers recombination (Eq. 23) and at high occupancy of the semiconductor particles by electron-hole pairs, trapping is a much slower process (Eq. 24). Herein we developed two kinetic models with considering the mentioned two states and then, the fitting of two models with experimental results was compared. With low h^+-e^-concentration assuming (Eq. 23), the concentration of photo-induced holes is described as:

$$[h^+] = \frac{k_1 I[ZnO]}{k_t} \quad (25)$$

By considering the high h^+-e^-concentration (Eq. 24):

$$[h^+] = \left(\frac{k_1}{k_2}\right)^{1/2} I^{1/2}[ZnO]^{1/2} \quad (26)$$

Now, by substituting Eqs. 25 and 26 in to Eq. 20 and combining the concentration of adsorbed hydroxyl radicals with Eq. 14, the rate equation could be ultimately described by the following Eqs. for low h^+-e^-concentration (LheC) and high h^+-e^-concentration (HheC) assumptions:

$$r_{D,LheC} = \frac{k' \frac{k_1 I[ZnO]}{k_{10}}}{1 + \left(\frac{k_7+k_8}{k_{10}}\right)[Dye]_{10} + \left(\frac{k_9 k_1}{k_{10} k_t}\right) I[ZnO]}[Dye] \quad (27)$$

$$r_{D,HheC} = \frac{k' \left(\frac{k_t}{k_{10}}\right) \left(\frac{k_1}{k_2}\right)^{1/2} I^{1/2}[ZnO]^{1/2}}{1 + \left(\frac{k_7+k_8}{k_{10}}\right)[Dye]_{10} + \left(\frac{k_9}{k_{10}}\right) \left(\frac{k_1}{k_2}\right)^{1/2} I^{1/2}[ZnO]^{1/2}}[Dye] \quad (28)$$

The above reaction rate equations could be reduced to the following form:

$$r_{D,LheC} = k_{app}[Dye] = \frac{\beta_{L,1} I[ZnO]}{1 + \beta_{L,2}[Dye]_0 + \beta_{L,3} I[ZnO]}[Dye] \Rightarrow k_{app} = \frac{\beta_{L,1} I[ZnO]}{1 + \beta_{L,2}[Dye]_0 + \beta_{L,3} I[ZnO]} \quad (29)$$

$$r_{D,HheC} = \frac{\beta_{H,1} I^{1/2}[ZnO]^{1/2}}{1 + \beta_{H,2}[Dye]_0 + \beta_{H,3} I^{1/2}[ZnO]^{1/2}}[Dye] \Rightarrow k_{app} = \frac{\beta_{H,1} I^{1/2}[ZnO]^{1/2}}{1 + \beta_{H,2}[Dye]_0 + \beta_{H,3} I^{1/2}[ZnO]^{1/2}} \quad (30)$$

Eqs. 29 and 30 represent the first-order kinetic constants related to the operational parameters including light intensity, initial dye concentration and ZnO content. The equations constants, $\beta_{L,i}$ and $\beta_{H,i}$, were calculated by linear least-squares method using Matlab 7.9 software and are given in Table 2. To compare the experimental k_{app} and calculated apparent rate constants, the correlation coefficient (R^2) values, sum of squared error (SSE) and root–mean–square error (RMSE) were obtained as the performance error functions. The SSE and RMSE values were calculated by following Eqs.:

$$SSE = \sum_{i=1}^{N} (y_{i,pred} - y_{i,exp})^2 \quad (31)$$

$$RMSE = \sqrt{\frac{1}{N} \sum_{i=1}^{N} (y_{i,pred} - y_{i,exp})^2} \quad (32)$$

In these equations, N is the number of data points and $y_{i,pred}$ and $y_{i,exp}$ are the predicted and experimental photodegradation efficiency, respectively. According to the results given in Table 2, the values of k_{app} calculated by HheC assumption model (Eq. 30) are in good agreement with experimental k_{app}.

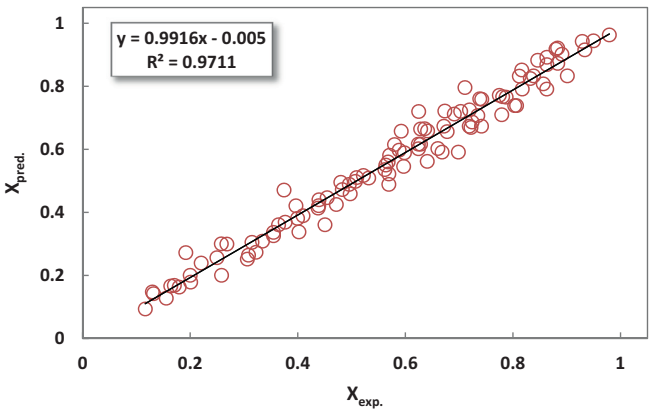

Fig. 4. Comparison of the experimental degradation efficiency with those calculated via developed kinetic model (Eq.33) with considering the high concentration of high h^+-e^- on ZnO nanoparticles.

Finally, by combining Eqs. 30 and 1, predicted degradation efficiency expression related to operational parameters is obtained as following:

$$X_{\text{pred}} = 1 - \frac{C}{C_0} = 1 - \exp(-k_{\text{app}}t) = 1 - \exp\left(-\frac{4.717 \times 10^{-4} I^{\frac{1}{2}} [\text{ZnO}]^{\frac{1}{2}}}{1 + 3.608 \times 10^{-2}[\text{Dye}]_0 - 2.49 \times 10^{-2} I^{\frac{1}{2}} [\text{ZnO}]^{\frac{1}{2}}} \times t\right) \quad (33)$$

In order to evaluate developed kinetic model, X_{pred} vs. X_{exp} was plotted (Fig. 4). It can be seen that the modeled data fit quite well with experimental data.

3.3. Empirical kinetic modeling of photocatalytic degradation

Based on the obtained results presented in Section 3.1, the photocatalytic degradation of AB9 followed from pseudo first-order kinetic and k_{app} was affected by the initial dye concentration, light intensity, pH and ZnO content. The non-linear relation between apparent first order rate constant and each of the mentioned parameters could be presented as the following power series model:

$$k_{\text{app}} = k_i x_i^{\alpha} \quad (34)$$

The comprehensive expression for k_{app} could be described as:

$$k_{\text{app}} = k_{\text{im}}[x_1]^{\alpha_1}[x_1]^{\alpha_1}\cdots[x_n]^{\alpha_n} \quad (35)$$

The model constants, k and α, were calculated for each parameter (x) by power series fitting of 120 items of experiments using Matlab 7.9 software and are listed in Table S2 of the supporting Information. The k_{im} is the mean of the calculated k_i values. Including the values of obtained constants in Eq. 35 results calculated k_{app}:

$$k_{\text{app}} = 0.001977[\text{AB9}]^{-0.9304}[pH]^{-0.7569}[\text{L.I}]^{0.9790}[\text{ZnO}]^{0.8856} \quad (36)$$

As a consequence, an empirical kinetic model for the photocatalytic degradation efficiency prediction was obtained by combining Eq. 1 and Eq.36:

$$X_{\text{pred}} = 1 - \frac{c}{c_0} = 1 - \exp(-k_{\text{app}}t) = 1 - \exp(-0.001977[\text{AB9}]^{-0.9304}[pH]^{-0.7569}[\text{L.I}]^{0.9790}[\text{ZnO}]^{0.8856} \times t) \quad (37)$$

The correlation between experimentally photocatalytic degradation efficiency and predicted ones shows good performance ($R^2 = 0.9821$) for developed empirical kinetic model (Fig. S2 of supporting information).

3.4. Artificial neural network developing for photocatalytic degradation of AB9

Artificial neural networks provide a facile method to obtain relationships between input variables (independent variables) and one or several output variables (dependent variables or responses). There are various types of neural networks used by researchers for different objects. Multilayer feed-forward type (multilayer perceptron, MLP) is the most popular in chemical processes, which consists of an input layer. Every network consists of one input layer, one or more hidden layers and one output layer. Firstly, input data, including values of inputs (descriptors), are presented to the nodes (multiple cells) of the input layer. Then, inputs are weighted by the connections (w_i) and results are added to bias (b_i) between the input and hidden layer. In the hidden layer, the weighted data are placed on a transfer function. In other words, each neuron in hidden layers, receives weighted inputs, sums them up and inserts the summation result in the transfer function to produce activation. The most common transfer function is sigmoid [35,36]:

$$f(x) = \frac{1}{1 + e^{-x}} \quad (38)$$

Again, the produced activations are weighted by the connections (w_j) and added to bias (b_j) between the hidden layer and output layer. Output nodes act as hidden neurons. They perform summation of weighted signals from the hidden layer and transfer them to transfer function, which is commonly the linear function. The output of the output layer is the predicted response [37]. This procedure is called forward pass (Eq. 39).

$$y_{\text{pred}} = f_{\text{pueline}}\left\{\sum_{j=1}^{m} w_j [f_{\text{tansig}}(\sum_{j=1}^{m}(x_i w_i + b_i)] + b_j\right\} \quad (39)$$

Where m and n are the number of neurons in hidden layer and input variable, respectively. The weights (w_i and w_j) and biases (b_i and b_j) are the adjustable parameters. The optimum values of weights and biases are obtained by iterative procedures called training. First, the initial random values are attributed to adjustable parameters, and then training starts with a forward pass through the training set of samples with related experimental response. At the end of the forward pass, the error between experimental and calculated response is determined. The error values are utilized to correct the previous weights and adjust all weights and biases in a step called backpropagation step. These forward and backpropagation steps form epochs. The forward and backpropagation steps are repeated until the minimum error between experimental and predicted responses is achieved.

In order to model the photocatalytic degradation of AB9 by ANN, a three layer MLP, with backpropagation algorithm was utilized. Initial AB9 concentration (over range of 10–30 mg/L), pH (4.3–11.3), ZnO content (50–125 mg/L), light intensity (8–16.3 W/m^2) and time (10–80 min) were the input variables and photocatalytic degradation efficiency was the output variable. Due to application of sigmoid function in hidden layer, all samples of input variables (x_i) were scaled in the 0.1–0.9 intervals by following Eq. [35,37]:

$$x_{\text{scaled}} = 0.1 + 0.8\frac{(x_i - x_{\min})}{(x_{\max} - x_{\min})} \quad (40)$$

A total 152 experimental data shuffled and split between training and test sets. The training and test sets included 92 and 60 data, respectively.

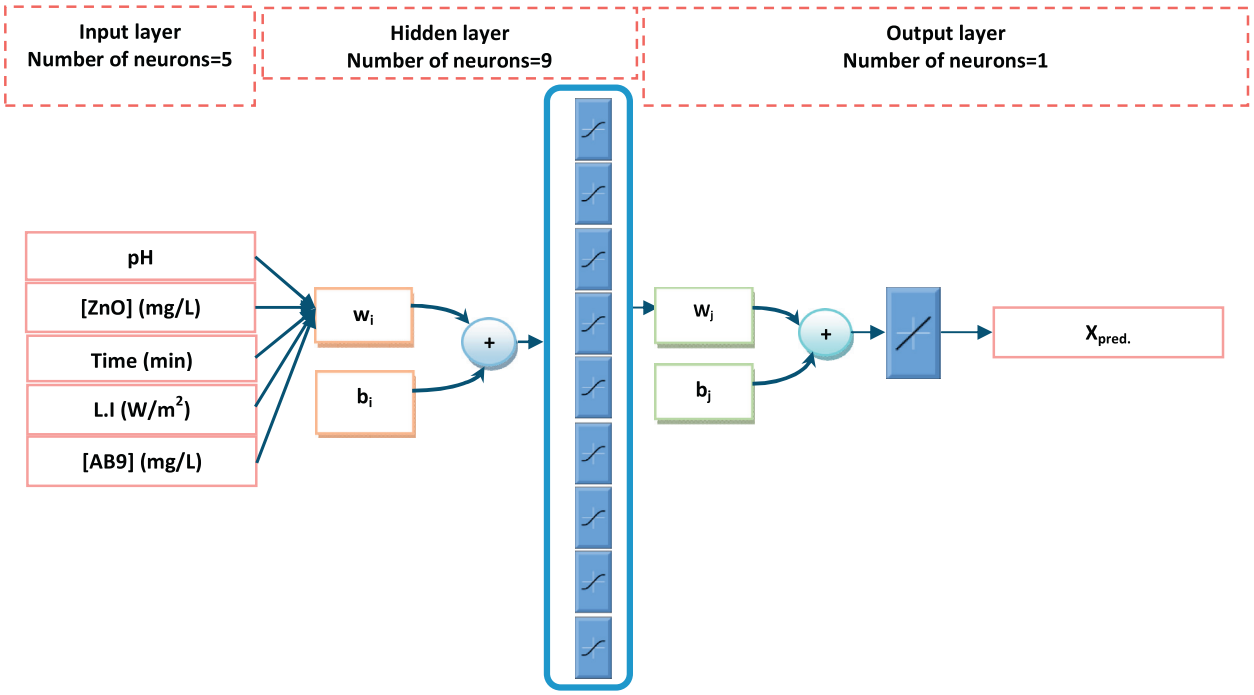

Fig. 5. The ANN optimum topology.

The topology of an ANN is specified by the number of layers and number of neurons in hidden layer. Theoretically, one hidden layer is enough for MLP neural networks [35]. Consequently, the three layer perceptron neural network with (5:N:1) architecture were developed. Number Five, N and one are the number of neurons in input, hidden and output layers. The number of neurons in input corresponded to the number of operational parameters. The number of output neurons corresponded to the photocatalytic degradation efficiency. The most important step in the optimization of ANN topology is the determination of the number of neurons in hidden layer. In this step, many three-layer perceptrons with different number of neurons in hidden layer (4–18) were trained by training set. Then, each developed ANN was evaluated using modeling of test set of data and calculating RMSE as an error function for test series. Based on the obtained results, it was found that the minimum RMSE equal to 0.03362 were achieved by inclusion of nine neurons in the hidden layer. Accordingly, based on the approximation of RMSE function, the optimum topology (Fig. 5) for photodegradation of AB9 modeling by MLP was (5:9:1). To test the precision of the developed ANN model, a comparison between experimental outputs and predicted outputs was performed by optimum MLP and provided optimum weights for an independent set of data (test set). The results (R^2 = 0.9884) confirmed that the ANN developed model predicts adequately the photocatalytic degradation efficiency (Fig. S3 of supporting information).

3.5. Comparison of developed kinetic, empirical kinetic and ANN models performance

The predictive capability of developed kinetic, empirical kinetic and ANN models for photodegradation efficiency prediction was evaluated using R^2, SSE and RMSE functions. The results presented in Table 3 shows that all developed models predict photocatalytic degradation efficiency with acceptable accuracy because of high values of R^2 and low SSE and RMSE. Also, it is found the better capability of ANN model than others because higher value of R^2 and lower error functions. To investigate more about the prediction capability of all three models, analysis of variance (ANOVA) was performed and obtained results are given in Table 4. It was found that there is no significant difference among the predicted photodegradation efficiencies by developed kinetic, empirical kinetic and ANN models. Consequently, the kinetic model is developed based on the determining elementary reactions, which occurred in photocatalytic degradation of AB9 by ZnO nanoparticles. In other words, because of adequate prediction of kinetic model and no significant difference with ANN prediction capability, the accurate reactions are involved in kinetic modeling. The accuracy of kinetic modeling depends on correct understanding about involved reactions and number of considered reactions in modeling while ANN model creates a correlation between experimental inputs and experimental outputs without any knowledge about the process phenomena. ANNs are able to retrieve general mechanism

Table 3
R^2, SSE and RMSE values for developed models.

Developed model	X_{pred}	R^2	SSE	RMSE
Kinetic	$1-\exp\left(-\frac{4.717\times10^{-4} I^{\frac{1}{2}}[\mathrm{ZnO}]^{\frac{1}{2}}}{1+3.608\times10^{-2}[\mathrm{Dye}]_0-2.49\times10^{-2} I^{\frac{1}{2}}[\mathrm{ZnO}]^{\frac{1}{2}}}\times t\right)$	0.9711	0.1578	0.0393
Emperical kinetic	$1-\exp(-0.001977[\mathrm{AB9}]^{-0.9304}[pH]^{-0.7569}[\mathrm{L.I}]^{0.9790}[\mathrm{ZnO}]^{0.8856}\times t)$	0.9821	0.1107	0.0306
ANN	Three layer perceptron with (5:9:1) topology	0.9883	0.0881	0.0242

Table 4
ANOVA calculation for difference among kinetic, empirical kinetic and ANN developed models.

Component	Source of variation	SS[a]	df[b]	MS[c]	*F*[d]	*P*-value	*F* crit.[e]
X_{pred}	Between models	0.002305	2	0.001153	0.022371	0.977878	3.019922
	Within models	19.21856	373	0.051524			
	Total	19.22086	375				

[a] Sum squared.
[b] Degree of freedom.
[c] Mean squared.
[d] *F* ratio.
[e] *F* critical.

and correct information from presentation of experimental inputs. Generally, ANN models give better estimation of process owing to stochastic manner and there is no need for mathematical description of reactions occurred in the process.

Acknowledgment

The authors are grateful to the Azarbaijan Shahid Madani University and University of Zanjan for financial supports.

References

[1] P. Roy, A.P. Periasamy, C.-T. Liang, H.-T. Chang, Environ. Sci. Technol. 47 (2013) 6688–6695.
[2] I. Udom, M.K. Ram, E.K. Stefanakos, A.F. Hepp, D.Y. Goswami, Mater. Sci. Semicond. Process. 16 (2013) 2070–2083.
[3] C.-C. Chen, H.-J. Fan, J.-L. Jan, J. Phys. Chem. C 112 (2008) 11962–11972.
[4] A. Mahyar, A.R. Amani-Ghadim, Micro Nano Lett. 6 (2011) 244–248.
[5] S.-Y. Lee, S.-J. Park, J. Ind. Eng. Chem. 19 (2013) 1761–1769.
[6] M. Motegh, J.R. van Ommen, P.W. Appel, M.T. Kreutzer, Environ. Sci. Technol. (2013).
[7] M. Goel, J.-M. Chovelon, C. Ferronato, R. Bayard, T.R. Sreekrishnan, J. Photochem. Photobiol. B: Biol. 98 (2010) 1–6.
[8] H. Fang, Y. Gao, G. Li, J. An, P.-K. Wong, H. Fu, S. Yao, X. Nie, T. An, Environ. Sci. Technol. 47 (2013) 2704–2712.
[9] A.M. Ali, A.A. Ismail, R. Najmy, A. Al-Hajry, J. Photochem. Photobiol. A: Chem. 275 (2014) 37–46.
[10] A.M. Ali, E.A.C. Emanuelsson, D.A. Patterson, Appl. Catal. B Environ. 97 (2010) 168–181.
[11] S.K. Pardeshi, A.B. Patil, J. Mol. Catal. A: Chem. 308 (2009) 32–40.
[12] E.R. Carraway, A.J. Hoffman, M.R. Hoffmann, Environ. Sci. Technol. 28 (1994) 786–793.
[13] M. Ahmad, E. Ahmed, Z.L. Hong, W. Ahmed, A. Elhissi, N.R. Khalid, Ultrason. Sonochemistry 21 (2014) 761–773.
[14] S. Ameen, M. Shaheer Akhtar, H.-K. Seo, H.-S. Shin, Mater. Lett. 113 (2013) 20–24.
[15] P. Amornpitoksuk, S. Suwanboon, S. Sangkanu, A. Sukhoom, N. Muensit, J. Baltrusaitis, Powder Technol. 219 (2012) 158–164.
[16] H. Bai, Z. Liu, D.D. Sun, Int. J. Hydrog. Energy 37 (2012) 13998–14008.
[17] H. Benhebal, M. Chaib, T. Salmon, J. Geens, A. Leonard, S.D. Lambert, M. Crine, B. Heinrichs, Photocatalytic degradation of phenol and benzoic acid using zinc oxide powders prepared by the sol–gel process, Alex. Eng. J. 52 (2013) 517–523.
[18] X. Cai, Y. Cai, Y. Liu, S. Deng, Y. Wang, Y. Wang, I. Djerdj, Ceram. Int. 40 (2014) 57–65.
[19] C.S. Turchi, D.F. Ollis, J. Catal. 122 (1990) 178–192.
[20] Y. Li, S. Sun, M. Ma, Y. Ouyang, W. Yan, Chem. Eng. J. 142 (2008) 147–155.
[21] D.F. Ollis, E. Pelizzetti, N. Serpone, Environ. Sci. Technol. 25 (1991) 1522–1529.
[22] M.B. Kasiri, H. Aleboyeh, A. Aleboyeh, Environ. Sci. Technol. 42 (2008) 7970–7975.
[23] O.B. Ayodele, H.S. Auta, N.M. Nor, Ind. Eng. Chem. Res. 51 (2012) 16311–16319.
[24] X.-H. Song, P.K. Hopke, Environ. Sci. Technol. 30 (1996) 531–535.
[25] G. Moradi, M. Mohadesi, M.R. Moradi, J. Pet. Sci. Technol. 108 (2013) 74–81.
[26] M.S. Seyed Dorraji, S. Aber, M.G. Hosseini, M. Raghibi-boroujeni, I. Ahadzade, Int. J. Nanotechnol. 6 (2009) 984–996.
[27] N. Daneshvar, S. Aber, M.S. Seyed Dorraji, A.R. Khataee, M.H. Rasoulifard, Sep. Purif. Technol. 58 (2007) 91–98.
[28] A.R. Khataee, V. Vatanpour, A.R. Amani Ghadim, J. Hazard. Mater. 161 (2009) 1225–1233.
[29] S. Dutta, S.A. Parsons, C. Bhattacharjee, P. Jarvis, S. Datta, S. Bandyopadhyay, Chem. Eng. J. 155 (2009) 674–679.
[30] R. Terzian, N. Serpone, J. Photochem. Photobiol. A: Chem. 89 (1995) 163–175.
[31] R. Terzian, N. Serpone, M.A. Fox, J. Photochem. Photobiol. A: Chem. 90 (1995) 125–135.
[32] A.R. Khataee, M. Fathinia, S. Aber, Chem. Eng. Res. Des. 89 (2011) 2110–2116.
[33] A.R. Khataee, M. Fathinia, S. Aber, Ind. Eng. Chem. Res. 49 (2010) 12358–12364.
[34] G. Rothenberger, J. Moser, M. Graetzel, N. Serpone, D.K. Sharma, J. Am. Chem. Soc. 107 (1985) 8054–8059.
[35] R. Nabavi, A. Niaei, D. Salari, J. Towfighi, J. Anal. Appl. Pyrolysis 80 (2007) 175–181.
[36] M. Sedighi, K. Keyvanloo, J. Towfighi, Ind. Eng. Chem. Res. 50 (2011) 1536–1547.
[37] F. Despagne, D. Massart, Analyst 123 (1998) 157R–178R.